Fabrication of a Semi-Active Controlled Friction Damper Device

Mitchell Stiles

Mentors: Liang Cao, James M. Ricles, Austin Downey, Safwan Al-Subaihawi, Simon Laflamme

University of South Carolina, College of Engineering and Computing
ATLSS Engineering Research Center, Lehigh University

1. Abstract

Applications of high performance damping devices can bring about cost-effective methods for mitigation of natural hazards. These devices have certain limitations in the areas of electrical reliability, mechanical robustness, and large resistance to force capabilities, so a second-generation is fabricated and will be tested in a semi-active controlled setup. The device, termed Semi-Active Banded Rotary Device (SABR-FD), has heightened applicability compared to other damping technologies due to its mechanical robustness, technological simplicity, and high damping performance. The mechanical principle behind the device is based on a band brake, which has a high amplification of the applied force, while allowing for a variable control force [1]. The fabrication process, theoretical calculations, and simulations of the SABR-FD is presented and experimentally verified by conducting characterization tests, subjecting the device to various harmonic loads of different frequencies. Results from numerical simulations have concluded that the new frame and base plate are of a sufficient stiffness when applying 2500 lbs. of damper force to each support. Also, modal analysis and theoretical calculations give a satisfactory buckling load for the structure-to-drum connection with a tensile critical force of 31,957.93 lbs. and a compression critical force of 61,603.937. The testing done in passive mode of the new system reaches 5 kips of damping force, and this will be applied to the device once it is converted to the semi-active mode after the electric actuators arrive at a later time.

2. Introduction

In recent years, tall civil structures have been constructed with decreased weight and increased flexibility. These lighter and more flexible structures are more susceptible to damaging inter-story drift caused by high-winds, earthquakes or a combination of the two. These multi-hazard events create challenges for designers when preparing for the next natural disaster, as their combined loads on the structure create complex loading conditions. Tornados, earthquakes, hurricanes, and other multi-hazard events have shown the absolute vulnerability of transportation structures and buildings [2]. Supplemental damping devices have been used as a solution to reduce structural vibrations caused by natural hazard events. Passive systems are widely used, but these devices are tuned to a specific setting, limiting the amount of effectiveness to other resonances. On the other hand, active damping devices are also an option, but require large power sources to operate [19]. These large power sources may not be available during the occurrence of a natural hazard, can be expensive to use during wind events, and have the possibility of destabilizing a system [1].

Semi-active devices provide a solution to overcome the tuning challenge and have been shown to increase excitation mitigation. They combine the benefits of both active and passive damping strategies because they are exclusively reactive. This means that they can change their mechanical properties to give more controllability while using a fraction of the required power to run an active device, but do not add energy into a system. These devices significantly enhance energy dissipation using low power [2]. Semi-active devices are communally broken down into four classes: variable stiffness [14, 15], variable orifices [16], variable fluid [17] and variable friction [18] devices.

Variable friction devices provide high energy dissipation by dissipating mechanical energy into thermal energy using a friction force that is controlled by an actuator to vary the normal force [1]. Different types of actuators used in variable friction devices include: pneumatic [3, 4], hydraulic [5], electromagnetic [6, 7], electromechanical [8, 9], and piezoelectric [10-13]. Despite their demonstrated benefit, semi-active friction damping devices have remained limited in application, possibly for their lower amounts of damping and unavailable commercial technologies. This work investigates a new semi-active device that relies on band brake technology to change the aspects of resonance mitigation. Having simple mechanics, different friction materials available, an adjustable resonance setting, and low maintenance costs of this device can expand the field of semi-active damping by providing a robust and damping technology with high-energy dissipation.

A recent design, the Banded Rotary Friction Device (BRFD), has be demonstrated in a passive configuration [1]. This project expands on this prior design by introducing controls to the device to create a semi-active friction damper, the SABR-FD. The purpose of this project is to introduce a third

generation of rotary variable friction devices with semi-active electric actuation to mitigate structural vibrations. In this paper, the SABR-FD is introduced, and a working prototype of the semi-active damper is tested and its response to harmonic excitation is reported. The research questions being asked are: (1) can a modulated friction damper with limited power reserves increase serviceability during multi-hazard events; and, (2) can a semi-active friction damper with electric actuators be used to meet serviceability requirements?

This paper is organized as follows. The next section will introduce the SABR-FD and its theoretical background (that of the BRFD). Theoretical background is followed by a presentation of a 3-stage dynamic model used to model the dynamic behavior of the device [1]. The sections afterwards discuss experimental methodology and the improvements made to the BRFD to create the SABR-FD along with the presentation and discussion of the experimental results. The final section is a conclusion which provides a summary of the findings from the project in its entirety.

3. Materials and Instrumentation

3.1 Materials

For the SABR-FD, A36 steel and stainless steel are used to produce a new brake drum for further experimentation on passive damping. This new drum has an increased width of 10 inches (previous drum was 8 inches wide). This drum also has rotating ball bearings to transmit the loads into the drum while eliminating moments from being transmitted into the drum. The new base design also uses A36 steel and is more structurally sound than the current setup. New support columns for the drum will raise the drum a total of six inches to allow room for the electric actuators. A drawing of the SABR-FD configuration with electric actuators is shown below in Figure 1.

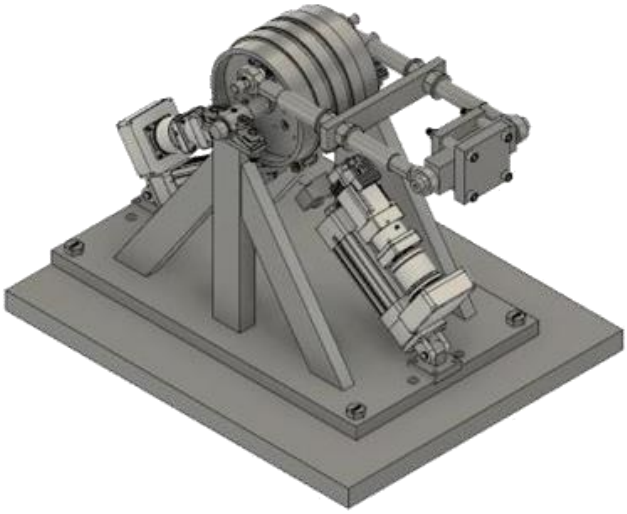

Figure 1: New Damper with New Base and Actuators

A structure-to-drum connection is also fabricated using A36 steel and Grade 8H 1.25” – 12 threaded rods (with nuts and washers). For testing purposes, this structure-to-drum connection is connected to a hydraulic actuator (MTS DuraGlide™ 244.22 Hydraulic Actuator). To remove moments in the connection, swivel rod ends are threaded to stainless steel rods. The other two rod ends are attached to a steel plate with 1”-8 socket screws. Figures 2 and Figure 3 below show the new drum in the current setup with the new structure-to-drum connection using the materials listed above.

Figure 2: New Steel Drum

Figure 3: New Connection with Threaded Rods

3.2 Software and IT

Software being used is mainly in the design phase of the project. Most modeling has been done in AutoCAD Fusion 360 and some in SolidWorks. Once the design is modeled, numerical simulations are run through Fusion 360 and some basic models are run through ABAQUS. Below in Figure 4, is an example of the new base plate being modeled and the associated modal frequencies, which finds frequencies that can cause dynamic amplifications and lead to yielding in the base plate material.

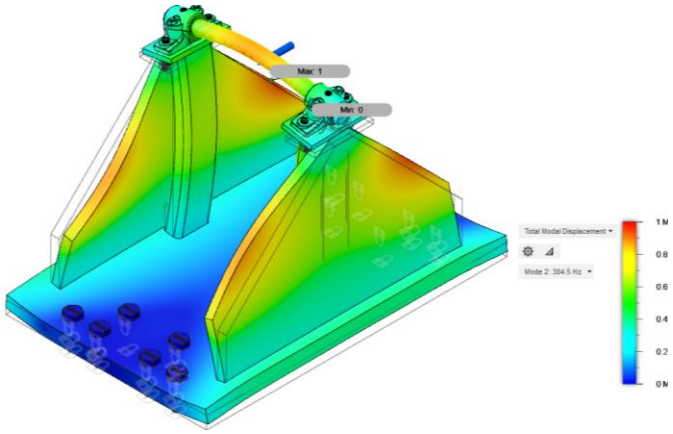

Figure 4: Modal Analysis of a New Base Design

One specific software called Pulsar is what is used to test the friction dampers in the laboratory. This software allows one to control the actuators that drive whatever is attached at the other end. Items such as frequency, load, stroke, and load can be measured and adjusted.

3.3 Instrumentation

There are a few instruments used while testing, like the MTS DuraGlide™ 244.22 Hydraulic Actuator, Transducer Techniques load cells, and the Tolomatic electric actuators provided by PennAir. The larger MTS actuator is connected to the friction drum and rotates the drum against the tensioned bands to generate the damping forces. The MTS actuator and new connection to the friction device can be seen in Figure 5 below (from left to right, is the I-beam connected to the back-end of the actuator, the actuator connection to the drum, then the SABR-FD).

Figure 5: Actuator-Friction Device Setup

The location of the first Transducer Techniques load cell in the current setup is shown to be underneath the screw jack to measure the amount of input force, $F_{applied}$, that is used to tension the friction bands. At the bottom of Figure 6, the load cell can be observed underneath the threaded rod, measuring the $F_{applied}$.

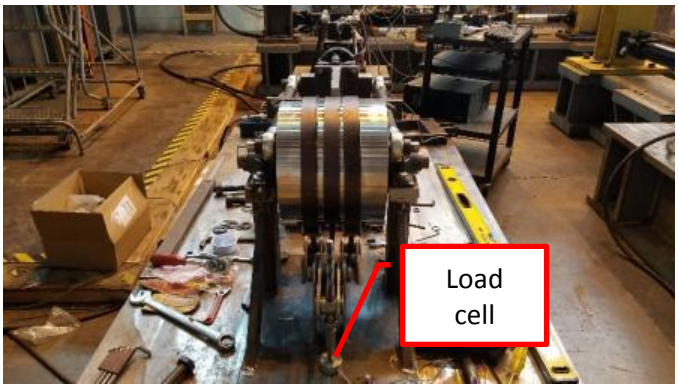

Figure 6: Load Cell Location

There is another load cell, but it is in the new base and connected to the electric actuators underneath

the drum. The load cell can be seen below in Figure 7, and the locations of the load cell allow the user to see the amount of tension in the bands and actuators at any given time. The last load cell is in the MTS actuator, and this one allows the user to see what stroke, frequency, and other components are occurring while the test is running in Pulsar. The load cells will be connected to a node box and will relay signals to the computer to read in Pulsar, effectively giving data needed to understand the friction model.

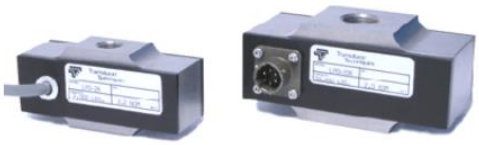

Figure 7: Transducer Techniques Low Profile Universal Actuator

Data acquired comes in from the load cells in the MTS actuator and can be displayed in different graphs. One of the main graphs that are important for understanding the friction damper is a damper force vs. displacement graph. An example of the graph is shown in Figure 8 below, where the damper hysteretic response (damper force-displacement from the damper rotating) is shown for three cases: (1) $F_{applied}$ = 50 lbs.; (2) $F_{applied}$ = 60 lbs.; and, (3) $F_{applied}$ = 70 lbs. The damper force capacity is shown to increase with a larger value for $F_{applied}$, which is due to the frictional force in the damper increasing with greater amounts of $F_{applied}$. Below the damper force-displacement graph is a damper force-velocity graph, which shows the velocity of the damper rotation.

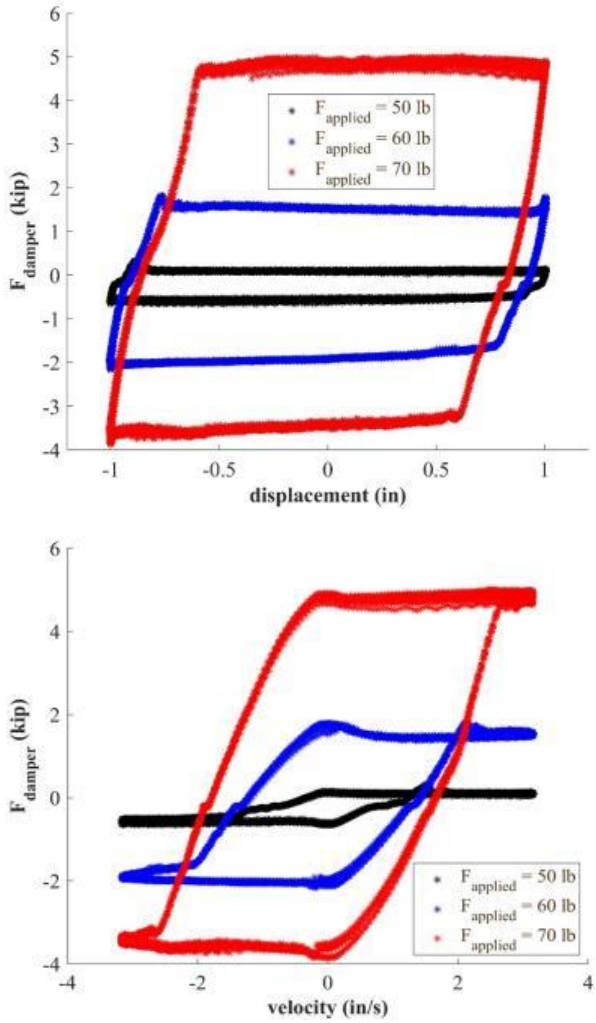

Figure 8: Force vs. Displacement and Force vs. Velocity

Electric actuators from Tolomatic are selected to start the process of creating the semi-active portion of the device. There are strict specifications needed for the actuator: needs to be able to hold 4000 lbs. maximum in tension, a brake to hold the load, a high ratio gearbox to assist the brake in holding the forces, a voltage requirement of 48VDC or lower, and the length must be less than 20 inches (so that it can fit into the design). Two specific Tolomatic part numbers are selected for each side of the drum to hold the forces in place. Figure 9 shows the CAD rendering of the Tolomatic electric actuator.

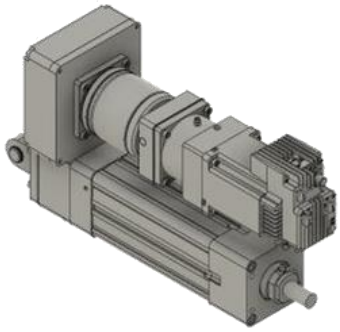

Figure 9: Tolomatic Electric Actuator

3.4 Friction Mechanism

The SABER-FD is mounted into a servo-hydraulic testing setup with an 11 kip capacity MTS actuator so characterization testing can be conducted. The damping mechanism for the drum is shown below. The band is anchored at one end, where the input force ($F_{applied}$) is applied to the center band, resulting in a reactionary force ($F_{reaction}$) at the opposite end. Once drum rotation occurs, the damper force (F_{damper}) derived from friction force is generated in the opposite direction of rotation [1]. The force represented is simply:

$$F_{reaction} = F_{applied} + F_{damper} \quad \text{[Eqn. 1]}$$

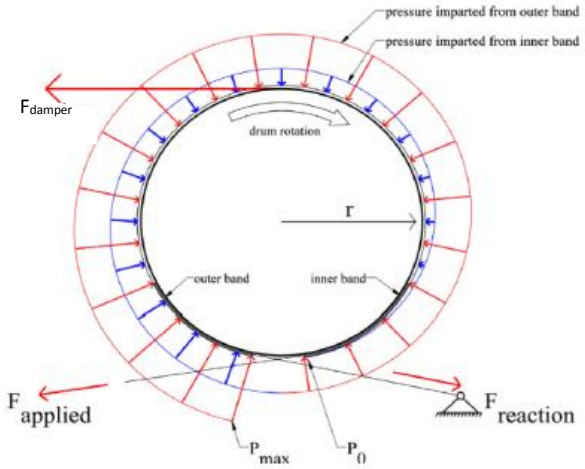

Figure 10: Forces Acting on the SABR-FD

4. Methodology

The methods involved within this project are in two stages: design and testing methods. First, designing the new drum is done and modeled using Fusion 360. This third-generation friction device takes a lot of the second-generation device ideas and improves upon them. Returning to Figure 2, the drum has more surface area than the previous drum, giving an option to increase the amount of friction that is in contact with steel surface. The drum also takes advantage of two 0.25 inch thick plates conveniently located 1.25 inches inward from the outer edge of the drum. A third plate is placed directly in the middle, reinforcing the drum when it is compressed by the bands. The plates are welded into place and a center rod is placed through the center so that the drum can mount to the top of the support towers in the pillow block bearings (seen in Figures 3 and 5).

After the drum is fabricated, the next step is modeling the new connection from the structure to the drum. The idea is using two threaded rods with rod ends on either end to transfer the load. Once the connection is created in Fusion 360, analyses of the connection needed to be tested using modal, buckling, and static analysis. These three tests show what frequencies and forces will yield the system based on the sizes and strength of the materials used. Figure 11 below shows the results from a buckling analysis of one of the beginning versions of the connection (newer versions are needed to satisfy a pin-to-pin connection, not a fixed-to-pin connection). This connection piece has 5000 lbs. applied to the back end, where it is attached to the actuator, and the force is transferred through the threaded rods to the pin connections on a machinable rod. The machinable rod is inserted into the drum, which connects the drum to the MTS DuraGlide™ 244.22 Hydraulic Actuator.

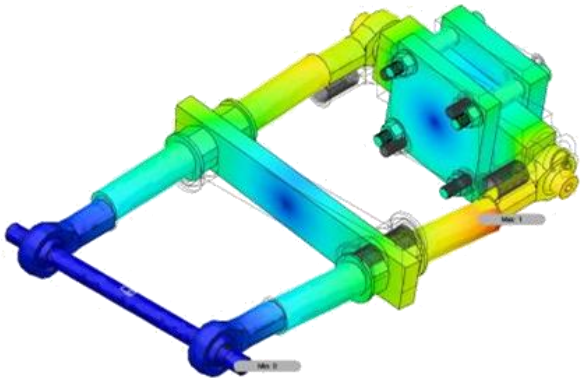

Mode Number	Frequency (Hz)
1	60.64
2	71.9
3	275.6
4	285.6
5	367.6

Figure 11: Structural Buckling Modes

Shear analysis is done on every part of the connections following the load path to better understand what parts need to be mechanically sound and what the maximum forces these parts can endure before yielding. The following calculations are done for buckling analysis on the connection. The first calculations are for tensile load (P_{all}) per rod.

$$P_{All} = 0.75 * F_{yield} * Area\ (rod) \quad \text{(Eqn. 2)}$$

Where F_{yield} is 128,800 lbs. [20] and A is the cross section A = πr^2 (r = 0.625 in):

$$P_{All} = 0.75 * 128{,}000 * \pi * 0.625^2 = 117{,}810\ lb_f$$

When in tension, 2500 lb_f will be traveling through each rod, giving a good factor of safety (62), so no tension failure will occur. The next calculation is compression on the threaded rods.

Compression buckling equation:

$$F_{CR} = \frac{\pi^2 * E * I}{(KL)^2} * \frac{1}{Factor\ of\ Safety} \quad \text{(Eqn. 3)}$$

Second moment of inertia equation:

$$I = \frac{\pi}{4} r^4 \quad \text{(Eqn. 4)}$$

Where: E is 30e6 psi, I (second moment of inertia) is $\frac{\pi}{4}(0.625)^4$, K is column effective length factor of a pin-pin connection (1.0), L is unsupported column length of 24 inches, and Factor of Safety is 1.92:

$$P_{All} = \frac{\pi^2 * 30e6\ psi * 0.11974\ in^4}{(1.0 * 24\ in)^2} * \frac{1}{1.92}$$

$$P_{All} = 32{,}085\ lb_f$$

When in compression, 2500 lb_f will be traveling through each rod, giving a large factor of safety (24.6), so no buckling will occur. In the new design, three foot threaded rods may need to be used, which will decrease the allowable force required to buckle the rods to 14,260 lbs. in compression. The rods will fail in tension with the same 117,810 lbs., so, the threaded rods won't buckle when put into the design. The rod ends have a static radial load capacity of 76,200 lbs. and the radial capacities for the rod ends won't increase beyond 2500 lbs. through each rod (factor of safety 24.6).

Shear and moment analysis ($V_{allowable}$ and $M_{allowable}$) are done for the center rod through the middle of the drum to see its capacities. The following calculations are done for the center rod with radius 0.75 inches and a yield strength of 36,000 psi for A36 steel.

Shear capacity equation:

$$V_{all} = 0.6 \text{ x } F_y \text{ x } A \quad \text{(Eqn. 5)}$$

Knowing the yield strength of A36 steel is 36,000 psi and the radius of the rod is 0.75 inches…

$$V_{all} = 0.6 \text{ x } 36{,}000 \text{ psi x } (\pi * (0.75in)^2)$$

$$V_{all} = 152{,}681\ lb_f$$

The maximum demand shear on the center rod is as follows:

$$V_{max} = 0.5 * P \quad \text{(Eqn. 6)}$$

Where P is the damping force of 5 kips.

$$V_{max} = 0.5 * 5000 = 2500\ lbs$$

Since V_{max} = 2500 lbs. < V_{all} = 152,681, the center rod won't shear. Next calculations are the moment capacity and maximum moment experienced by the center rod. The moment capacity equation is as follows:

$$M_{all} = 0.75 \text{ x } F_y \text{ x } S \quad \text{(Eqn. 7)}$$

First, section modulus (S) for a circle is:

$$S = \frac{\pi r^3}{4} \quad \text{(Eqn. 8)}$$

$$\text{So, } S = \frac{\pi(0.75)^3}{4} = 0.33134\ in^3$$

$$M_{all} = 0.75 \text{ x } 36{,}000 \text{ psi x } 0.33134 \text{ in}^3$$

$$M_{all} = 8946\ lb_f * in.$$

The maximum demand moment on the center rod is as follows:

$$M_{max} = P * L \quad \text{(Eqn. 9)}$$

Where P is the damper force (from one of the threaded rods) and L is the length of the center rod from the point load to the welded outer plate.

$$M_{max} = 2500 * 3 = 7500\ lb_f * in.$$

Since M_{max} = 7500 lbs.-in. < M_{all} = 8946 lbs.-in., the center rod won't reach its allowable moment capacity.

The final design element is the base drawing and fitting the electric actuators in place. Simulations are being conducted to see what thicknesses of steel plates work for the base, what bracket thickness is needed for the support columns, and where bolts need to be placed for maximum stiffness so little elastic bending occurs. Figure 4 is a good example of what analysis is being done to see how the steel plate base reacts to the force from the actuator being distributed to each support column.

The testing method is relatively simple, as it does not require much setup and detail to run a successful test. The SABR-FD is mounted into a servo-hydraulic testing setup with an 11 kip capacity MTS actuator and characterization testing is conducted. Referring to Figure 5, the test setup can be observed to see where everything is laid in line relative to the back end of the MTS actuator. Applied forces in the current setup are controlled via a screw jack that tensions the band with a threaded rod when pushing up on the other end of the screw jack with a nut threaded onto a rod mechanism. This force of pushing the screw jack up is measured in the load cell located between the base plate and the rod mechanism. As stated earlier, the damping force generated is measured with a load cell located in the head of the MTS actuator. For the current setup, the damping force capacity F_{damper} is set at 5 kips (22.5 kN) with a new friction material. This is done so that the current setup can be related to the soon-to-be semi-active setup. Having too high of a force for a working design requires large electric actuators, which won't fit within the size restraints of the new design.

The SABR-FD is subjected to displacement-controlled harmonic excitations having 1 inch amplitude at five different frequencies: 0.2, 0.5, 1.0, 2.0, and 3.0 Hz. Three different applied forces are investigated: 5 (22.24 N), 15 (66.72 N), and 25 lbs. (11.21 N), where 5 lbs. is the minimum force available from the actuation mechanism and 25 lbs. corresponds to the device's set maximum of 5 kips. Three tests per harmonic frequency is most desirable.

The passive mode of the SABR-FD is further validated using nonstationary excitations, which consists of six different seismic excitation tests. The tests are listed as follows: DBE Duzce, MCE Duzce, DBE Kocaeli, MCE Kocaeli, DBE Impvall, and MCE Impvall (DBE: Design Based Earthquake with 10% probability of exceedance in 50 years; MCE: Maximum Considered Earthquake with 2% Probability of exceedance in 50 years).

5. Preliminary Results

Research questions asked previously won't be answered until the device is configured to the semi-active mode. This will occur after this paper is written and will happen soon. Results from the design fabrication come from analyses on the base, frame, and structure-to-drum connection. Different designs for the frame are considered and simulated in Fusion 360. These different designs are subject to 2500 lbs. of pulling force and pushing force on each

column support. The other two forces are the two tension forces generated from the electric actuators that will be mounted to the base with clevis receivers. One side is experiencing 3250 lbs. of force, while the other will be experiencing around 100 lbs. of applied force. Below is the final design concept simulation of the frame and base plate with the forces described above.

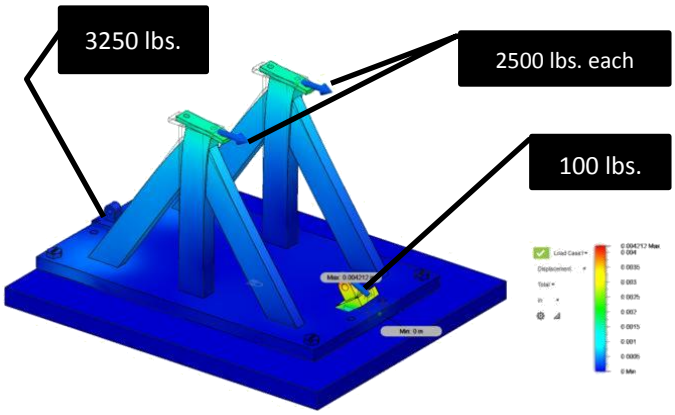

Input Force	Displacement
2500 lbs. (right support)	0.00198 in.
2500 lbs. (left support)	0.00203 in.
100 lbs. (front clevis)	0.00421 in.
3250 lbs. (rear clevis)	0.05 in.

Figure 12: Final Design of New Frame

The base plate deflects a maximum of 0.0002 inches (upwards) and the columns will displace 0.0019 inches in the direction of force acting on the support. These final parts will be fabricated and assembled after this report is completed.

The device will be implemented with the MTS DuraGlide™ 244.22 Hydraulic Actuator and a new sliding bearing block because the setup will be around eight inches taller. The reason for using this actuator is because the 11 kip actuator being used now is significantly longer, limiting the space for the friction damper. The 22 kip actuator ensures there is plenty of room for the base of the new SABR-FD. Figure 13 shows how the SABR-FD and MTS DuraGlide™ 244.22 Hydraulic Actuator will be mounted on the foundation beam.

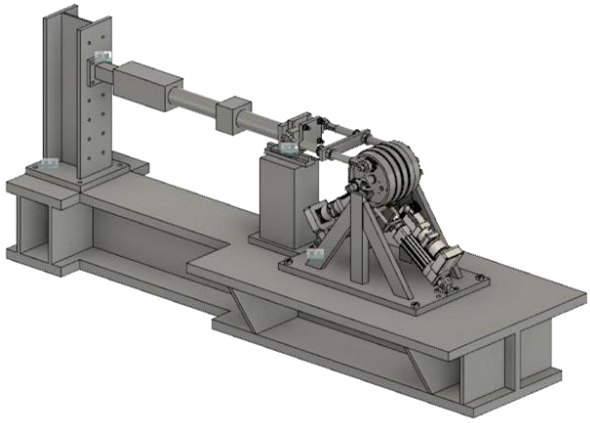

Figure 13: I-Beam Foundation with SABR-FD

6. Summary and Conclusions

In this report, a variable friction damper for structural control applications is presented. The device, termed Semi-Active Banded Rotary Friction Device (SABR-FD), is based on band brake technology and is a mechanically robust system with semi-active damping capabilities. This semi-active system will be proven effective once the electric actuators are inputted into the passive design.

This third generation device derived from the Banded Rotary Friction Device (BRFD) is fabricated and is subject basic characterization testing with further testing in hybrid simulations. The SABR-FD is tested in passive mode with new friction material (on the bands) under harmonic loads at different frequencies and applied loads. The device is capable of 5 kips of damping and will be tested in semi-active mode with the same specifications that are listed with the passive mode. The passive mode of this device will also be subjected to nonstationary excitations consisting of earthquake time series.

This third generation device's fabrication and testing further advances the possibility of future implementation of semi-active friction devices into structural applications. The SABR-FD is a third generation rotary damping systems designed from previous models created by others involved in this research. This device is specifically engineered to stiffen elements from previous designs and start the pursuit of semi-active friction damping using electric actuation. The SABR-FD has been drawn, simulated, fabricated, and completed some basic testing, validating its design and principle for

bringing about semi-active friction damping devices.

7. Acknowledgements

This material is based upon work supported by the National Science Foundation under Grant No. NSF-CMMI-1612144I.

Special thanks to Dr. Liang Cao and Dr. James Ricles for their commitment, time, and guidance throughout the summer NHERI REU (Natural Hazards Engineering Research Innovation Research Experiences for Undergraduates program). Also, to the supervisors in the ATLSS Engineering Research Facility for teaching important laboratory skills and fabrication of parts. Finally, Dr. Karina Vielma for her support throughout the summer.

8. References

[1] Downey, A., Cao, L., Laflamme, S., Taylor, D., and Ricles, J. (2016). "High capacity variable friction damper based on band brake technology." *Engineering Structures*, 113, 287-298.

[2] Cao, L., Downey, A., Laflamme, S., Taylor, D., and Ricles, J. (2015). "Variable friction device for structural control based on duo-servo vehicle brake: Modeling and experimental validation." *Journal of Sound and Vibration*, 348, 41–56.

[3] Vesselenyi, T., Dzitac, S., Dzitac, I., Manolescu, M-J. (2007). "Fuzzy and neural controllers for a pneumatic actuator." *International Journal of Computers Communication & Control*, 2(4), 375-387

[4] Mehmood, A., Laghrouche, S., and Bagdouri, M. E. (2011). "Modeling identification and simulation of pneumatic actuator for VGT system." *Sensors and Actuators A: Physical*, 165(2), 367–378.

[5] Kannan, S., Uras, H. M., and Aktan, H. M. (1995). "Active control of building seismic response by energy dissipation." *Earthquake Engineering & Structural Dynamics*, 24(5), 747–759.

[6] Lorenz, M., Heimann, B., and Härtel, V. (2006). "A Novel Engine Mount with Semi-Active Dry Friction Damping." *Shock and Vibration*, 13(4-5), 559–571.

[7] Yang, J. N., and Agrawal, A. K. (2002). "Semi-active hybrid control systems for nonlinear buildings against near-field earthquakes." *Engineering Structures*, 24(3), 271–280.

[8] Narasimhan, S., and Nagarajaiah, S. (2006). "Smart base isolated buildings with variable friction systems: H∞ controller and SAIVF device." *Earthquake Engineering & Structural Dynamics*, 35(8), 921–942.

[9] Kawamoto, Y., Suda, Y., Inoue, H., and Kondo, T. (2008). "Electro-mechanical suspension system considering energy consumption and vehicle manoeuvre." *Vehicle System Dynamics*, 46(sup1), 1053–1063.

[10] Chen, C., and Chen, G. (2004). "Shake table tests of a quarter-scale three-storey building model with piezoelectric friction dampers." *Structural Control and Health Monitoring*, 11(4), 239–257.

[11] Lu, L.-Y., and Lin, G.-L. (2008). "A Theoretical Study on Piezoelectric Smart Isolation System for Seismic Protection of Equipment in Near-fault Areas." *Journal of Intelligent Material Systems and Structures*, 20(2), 217–232.

[12] Durmaz, O., Clark, W. W., Bennett, D. S., Paine, J. S., and Samuelson, M. N. (2002). "Experimental and analytical studies of a novel semi-active piezoelectric coulomb damper." *Smart Structures and Materials: Damping and Isolation*, Proc. SPIE 4697, 258-273.

[13] Xu, Y. L., and Ng, C. L. (2008). "Seismic Protection of a Building Complex Using Variable Friction Damper: Experimental Investigation." *Journal of Engineering Mechanics*, 134(8), 637–649.

[14] Liu, Y., Matsuhisa, H., and Utsuno, H. (2008). "Semi-active vibration isolation system with variable stiffness and damping control." *Journal of Sound and Vibration*, 313(1-2), 16–28.

[15] He, W. L., Agrawal, A. K., and Mahmoud, K. (2001). "Control of Seismically Excited Cable-

Stayed Bridge Using Resetting Semiactive Stiffness Dampers." *Journal of Bridge Engineering*, 6(6), 376–384.

[16] Yang, J. N., Bobrow, J., Jabbari, F., Leavitt, J., Cheng, C. P., and Lin, P. Y. (2007). "Full-scale experimental verification of resetable semi-active stiffness dampers." *Earthquake Engineering & Structural Dynamics*, 36(9), 1255–1273.

[17] Yoshida, O., and Dyke, S. J. (2004). "Seismic Control of a Nonlinear Benchmark Building Using Smart Dampers." *Journal of Engineering Mechanics*, 130(4), 386–392.

[18] Spencer, B. F., and Nagarajaiah, S. (2003). "State of the Art of Structural Control." *Journal of Structural Engineering*, 129(7), 845–856.

[19] Ikeda, Y. (2004). "Active and Semi-Active Control Of Buildings in Japan." Journal of JAEE Journal of Japan Association for Earthquake Engineering, 4(3), 278–282.

[20] "Alma Bolt Company & Prime Fasteners 1-800-526-2200." (n.d.). Proof Load Tensile Strength for Grade 2, 5, & 8, <https://www.almabolt.com/pages/catalog/bolts/proofloadtensile.htm> (Jul. 30, 2019).